THESIS TITLE

by

Kara Kundert

A thesis submitted in partial satisfaction of the

requirements for the degree of

Master of Astrophysics

in

Astronomy

in the

Graduate Division

of the

University of California, Berkeley

Committee in charge:

Professor Aaron Parsons, Chair
Professor Martin White
Professor Eugene Chiang

Fall 2018

The thesis of Kara Kundert, titled THESIS TITLE, is approved:

Chair _____ Date _____

_____ Date _____

_____ Date _____

University of California, Berkeley

THESIS TITLE

Abstract

THESIS TITLE

by

Kara Kundert

Master of Astrophysics in Astronomy

University of California, Berkeley

Professor Aaron Parsons, Chair

In this memo, we seek to lay out a case for the use of absorber in an interferometric study of the spatial monopole of the 21cm reionization signature (i.e. the "global signal"). As discussed in previous memos, we believe that the way to optimize the sensitivity to the monopole term comes from the use of absorptive walls between the antennas to impose an artificially high "horizon", or temperature discontinuity, onto the beam of each antenna, thereby pushing the monopole into higher order spatial terms (Kundert 2016). With the new simulation, we are able to manipulate many parameters of our virtual interferometer, including but not limited to the antenna spacing, absorber wall height, and the attenuating properties of the absorber itself. From our exploration of these parameters, we are able to now state with certainty that we are able to detect the monopole term of the sky using a classical interferometer.

To DEDICATED PERSON

This is the dedication.

Contents

List of Figures

List of Tables

Acknowledgments

These are the acknowledgements.

Chapter 1

Introduction

very quick overview of HYPERION and breakdown of what's in each chapter

Chapter 2

The Global Signal – Its Physics and Significance to Cosmology

2.1 Overview of the Epoch of Reionization

In brief, the Epoch of Reionization refers to the period of the universe's history during which its supply of intergalactic hydrogen became reionized. This is important to its evolution, and therefore of interest to astronomers, due to the driving factor of that ionization: the ignition of the first stars, galaxies, and black holes in the universe. A positive detection of the Epoch of Reionization will help astronomers to clarify many open questions of cosmology, such as the properties of the first galaxies, how stars with zero metallicity formed, the physics of early quasars, and more.

In slightly more detail, let us begin at the beginning. At the start of time, the universe was extremely hot and ionized from the Big Bang. Over time, as space itself expanded and the gas within the universe cooled adiabatically along with that expansion, the temperature of the universe dropped low enough that the nearly uniform ionized plasma that made up the universe was able to recombine to form neutral hydrogen. This phase transition, which occurred approximately 380,000 years after the Big Bang, enabled photons to decouple from the baryonic matter, allowing photons to stream freely for the first time in the history of the universe. Those photons are what we now know as the "Cosmic Microwave Background" (CMB).

At the point of the CMB, the gravitational force had heretofore always served as second fiddle to the electromagnetic force, and the formation of structure was driven solely by dark matter (Zaroubi 2012). As such, structure had yet to form, and the release of the CMB led to a period known as the "Dark Ages" – a time when the universe had nothing to do but slowly get to work allowing slight matter over-densities to grow and transform into stars, galaxies, and black holes.

So, about 100 million years passed and the universe bathed in nothing but the after-glow of the Big Bang. Finally, the first galaxies formed, and along with them bright stars to

emit ionizing radiation. Soon, we find small ionized bubbles in the intergalactic medium (IGM), the hydrogen gas filling the space between galaxies. Over time, more galaxies and their bright stars make more ionized bubbles, until eventually the entire universe's supply of loose hydrogen gas has been converted into a proton-electron ionized plasma.

This period, very creatively, is called the Epoch of Reionization – the epoch during which the universe once again became ionized, like it was at the dawn of time.

As of yet, there has been no confirmed[1] direct detection of this time period – either of the objects that drive it nor of the gas behavior itself. This is not for lack of trying. There are currently (or soon to be) observatories looking for high-redshift galaxies and quasars (Gardner 2006), for power-spectrum measurements to find ionized regions around those high-energy objects (DeBoer 2017), and for the microscopic temperature changes in the gas of the universe (Bowman & Rogers 2010). As it turns out, these observations are hard to make – 13 billion light years is a long way for light to travel.

For the sake of brevity and intellectual focus, this thesis (and the experiment proposed within) will be focusing solely on observing the overall average behavior of the intergalactic medium as it evolves throughout this time period. This is referred to as the "global signal".

2.2 Overview of the Global Signal

The global signal of reionization is an observation of the overall average nature of hydrogen throughout this epoch, i.e. the spatially averaged signal from the neutral hydrogen gas, as observed using redshifted 21 cm emission from the intergalactic medium 13 billion years ago. More specifically, global signal experiments seek to observe the relationship between the internal level populations of the neutral hydrogen IGM and the ambient temperature of the universe, as set by the CMB photons. This relationship is written quantitatively in Eq. (2.1).

$$\delta T_b = (T_s - T_\gamma)(1 - e^{-\tau}) \tag{2.1}$$

where δT_b is the observed fluctuation in the 21 cm brightness temperature of the 21 cm line (T_s) relative to the background CMB brightness temperature (T_γ), and τ is the optical depth of the hydrogen through which the CMB is passing.

By observing the evolution of the spin temperature relative to the CMB background temperature, we are able to better understand how and when energy was injected into the gas (Pritchard & Loeb 2010). For example, the X-rays generated by black holes contributed to the heating of the gas, making the gas itself brighter than the ambient photons. Additionally, Lyman-α photons from Population II and III stars modify the coupling of the IGM gas temperature to the 21 cm spin temperature via the Wouthuysen-Field effect, providing a means to track early star formation (Furlanetto et al. 2006).

[1]While there has yet to be a confirmed direct detection of the Epoch of Reionization, the EDGES experiment has announced a possible detection of the 21 cm reionization global signal (Bowman et al. 2018).

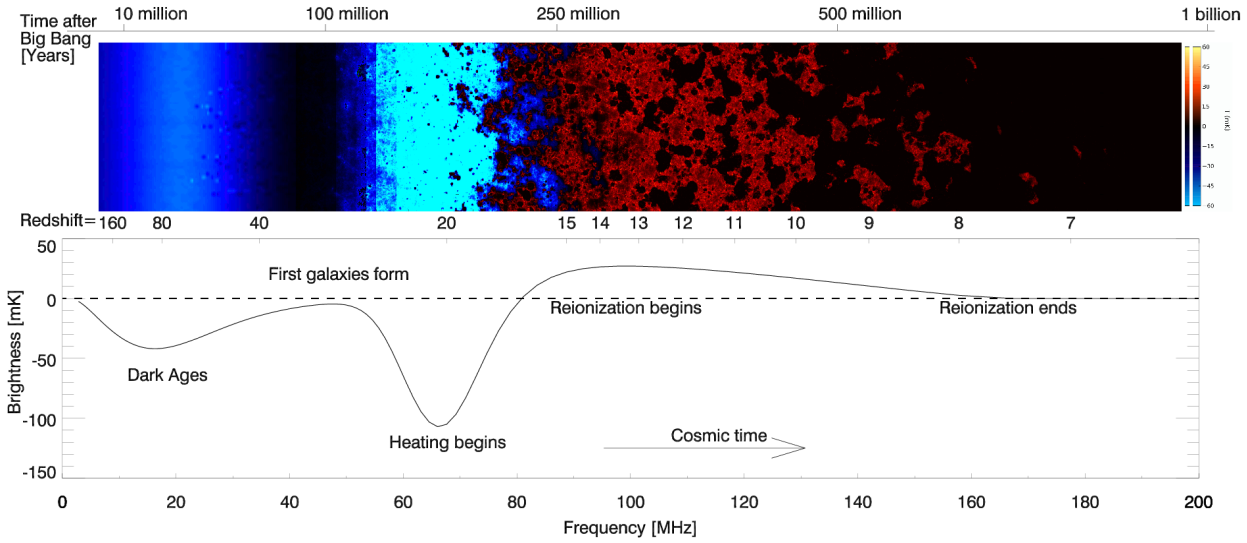

Figure 2.1: In the top half of the figure, we see a cartoon of the reionization history of the universe and the development and growth of ionized bubbles over time. In the bottom half, we see a breakdown of T_b, the brightness temperature of the 21 cm global signal, over time. There are five labeled regimes to this plot, each corresponding to the dominance of a different variable in the production of the 21 cm signal. Figure originally published in Pritchard & Loeb 2012.

However, while it's fairly straightforward to observe the 21 cm signal and acquire a measurement of the spin temperature through time, that alone doesn't give us much insight into the driving physics of that signal. First, we must understand what factors contribute to the spin temperature of the gas.

The spin temperature (T_s) is a function of five main variables – the thermal temperature of the hydrogen gas (T_K), the background temperature of the CMB photons (T_γ), the volume-averaged ionized fraction of hydrogen (x_i), the specific flux of the Lyman-α frequency (J_α), and the number density of hydrogen (n_H). There are six main physical regimes believed to have taken place during the process of structure formation and IGM reionization, which can be seen in Fig. 2.1 and are physically detailed below.

Brief History of the Global Signal

– ($200 \leq z \leq 1100$): During this time period, the residual free electron fraction remaining post-recombination and the high gas density allows the thermal and spin temperatures of the gas to remain coupled with the photon background via Compton scatting and collisional excitations. All temperatures are the same, and therefore there will be no detectable 21 cm signal.

- $(40 \leq z \leq 200)$: As cosmological expansion continues, Compton scattering no longer couples the thermal temperature of the gas to the CMB photons, and the gas and radiation decouple and go out of equilibrium. Collisional coupling sets the spin temperature $T_S < T_\gamma$, leading to an absorption feature in the 21 cm global signal.

- $(30 \leq z \leq 40)$: Expansion continues and collisional interactions are no longer effective at coupling the thermal and spin temperatures of the gas. The excitation levels shift to being set by radiative coupling to the CMB, such that $T_S = T_\gamma$, and there is no detectable 21 cm signal.

- $(15 \leq z \leq 30)$: As the first sources (e.g. stars, active galactic nuclei (AGN), etc...) ignite, they begin emitting high energy Lyman-α and X-ray photons. The hyperfine populations couple to the thermal temperature of the cold gas via the Wouthuysen-Field effect, such that $T_S \sim T_K < T_\gamma$, resulting in an absorption feature in the 21 cm global signal.

- $(7 \leq z \leq 15)$: The radiation (particularly the X-rays) from bright sources heat the gas, $T_K > T_\gamma$ and we see 21 cm emission in the global signal. Lyman-α coupling is still effective at setting the level populations.

- $(z \leq 7)$: Enough ionizing radiation has spread throughout the universe that the IGM has been converted from neutral to ionized, and reionization is complete.

At present, all redshift ranges listed are theoretical, as no confirmed detections have yet been made. However, it is abundantly clear that detection and study of this era of this part of the universe's history is rich with information about our cosmological origins, and could fill many of the gaps in our current knowledge.

Chapter 3

Interferometry

3.1 Brief Overview

Let's start with what they are. An interferometer is any device which superimposes the waves from a coherent light source in order to gain information about the source itself. So what does that mean? Let's look at the most basic case of a Michelson interferometer. In this scenario, we have a coherent light source (typically a laser) pointing at a beam splitter. The splitter splits the light into two identical beams, which travel on separate paths, until they are recombined before entering a detector. The difference in the paths creates a phase difference between the beams. This phase difference is what creates an interference pattern, which is what then gives us the information we seek about the light source, which typically comes in the form of fringes.

What if instead of using mirrors and beam splitters, we built two identical small telescopes that were physically separated in space, then pointed them at the same astronomical source. Because they're not in the same spot but are separated by a "baseline", there must be a difference in the path lengths between the telescopes and the source. This is the fundamental idea behind radio interferometers. Now let's explore the mathematics.

In order to get a handle on the mathematics and theory behind astronomical interferometry, we're going to make some simplifying assumptions. We will consider the case of a two-element interferometer (that is, an interferometer with two antennas and one "baseline" between them) observing a very distant source (so the emissions from the source will come in the form of plane waves and the antennas will point in the same direction on the sky). This interferometer will be fixed in space - so, no rotation or motion of the antennas themselves. We will also be looking at just one frequency, so the signals coming in will be perfectly sinusoidal with one known wavelength. We won't be worrying about anything in the backend, so we'll say that we have no frequency conversions (an RF interferometer) with a single polarization and perfectly idealized electronics (perfectly linear, no amplitude or phase distortions, perfectly identical for both instruments, and no added noise). We'll also assume no propagation distortions, so the plane waves we observe from the source won't be

disturbed by the ionosphere or atmosphere of Earth, and that the source is small enough in angular size that we can approximate the sky as flat and two-dimensional.

What does that leave us? Two identical sensors that are separated by a vector distance $\mathbf{b}$ - this is our baseline. These sensors are both pointed at a quasi-monochromatic source of frequency ν, in the vector direction $\mathbf{s}$. Combining these fundamental numbers, we then get the key quantity $\tau_g = \mathbf{b} \cdot \mathbf{s}/c$, which is the geometric time delay. That's the extra time needed for the signal to reach the more distant antenna. This number will be important to us in order to correlate our signals. We can also find the phase shift in the signal by writing $\Theta = \omega\tau_g = 2\pi\mathbf{b} \cdot \mathbf{s}/\lambda$.

With this knowledge of the phase difference between the paths, we can write out the voltages received by each of the sensors, so we get $V_1 = E\cos[\omega(t - \tau_g)]$, because it has that extra phase delay from the baseline separation, and $V_2 = \cos(\omega t)$. In this case, the path lengths from the sensor to the multiplier are treated as being equal, so we don't need to add any extra phase terms. We then multiply our signals together, and take an average over time, which gives us an averaged product $R_C = P\cos(\omega\tau_g)$. This quantity is dependent on the received power $P = E^2/2$ and the geometric delay τ_g, and hence on the baseline orientation and source direction. We can rewrite R_C to make this relationship more explicit as:

$$R_C = P\cos\left(2\pi\frac{\mathbf{b} \cdot \mathbf{s}}{\lambda}\right) \tag{3.1}$$

Note that R_C is not a function of the time of the observation (so long as the source itself is not transient or variable), the physical location of the baseline (provided that the source is in the far field, which is always true of astronomical sources), or the actual phase of the incoming signals. All that matters is the relative phase between the sensors!

In order to get a better understanding of our observed response, let's rewrite some terms. Let us say that $\mathbf{b} \cdot \mathbf{s}/\lambda = u\cos\alpha = u\sin\theta = ul$. In this case, we are defining

$$u \equiv b/\lambda \tag{3.2}$$

which is the baseline length in units of wavelengths, and θ is the angle relative to the zenith. $l = \cos\alpha = \sin\theta$ is the direction cosine. We can then rewrite our response function as $R_C = P\cos(2\pi ul)$. We can now see quite easily that the longer the baseline, the more rapid the frequency of the response function R_C. This is what radio astronomers call "fringes".

We can also begin to see why we want to have many sets of antennas - each baseline will only give us information about one set of fringes. In order to reconstruct a full image of an extended source, we need to be able to observe more than one spatial frequency. The response from an extended source is obtained by summing the responses at each antenna to all emission over the sky, multiplying the two for each pair of antennas, and averaging. Assuming that the source itself is spatially incoherent (e.g. that the emission from one side of the galaxy isn't related to the emission from the other side), the averaging and integrals can be interchanged, giving us

$$R_C = \iint I_V(\mathbf{s}) \cos(2\pi\nu \mathbf{b}\cdot\mathbf{s}/c) d\Omega \tag{3.3}$$

We can now see the relationship between what we are measuring to what we want to observe - we have linked the source brightness $I_V(\mathbf{s})$ to the even interferometer response R_C. To complete the image of the sky, we can observe the odd interferometer response R_S, which is the sinusoidal equivalent of R_C, by slipping in a 90° phase offset along one of the signal paths.

Now we can define a complex function $V = R_C - iR_S = Ae^{-i\phi}$ as our complex visibility from the two independent, real correlator outputs R_C and R_S, where $A = \sqrt{R_C^2 + R_S^2}$ and $\phi = \tan^{-1}(R_S/R_C)$.

We can now rewrite the complex visibility as an integral, giving us:

$$V_\nu(\mathbf{b}) = R_C - iR_S = \iint I_V(\mathbf{s}) e^{-2\pi i\nu \mathbf{b}\cdot\mathbf{s}/c}\, d\Omega \tag{3.4}$$

This is easily recognized as the 2D Fourier transform, when the right geometry is utilized. As it turns out, the earlier definitions of u and l are very convenient coordinates to use, and can be expanded to two dimensions to give us the (u, v) visibility plane and the (l, m) source plane. Eq. (5.1) can be rewritten with these coordinates like so:

$$V(u,v) = \iint I(l,m) e^{-2\pi i(ul+vm)}\, dl\ dm \tag{3.5}$$

This is the van Cittert-Zernike theorem, a fundamental equation for interferometry, which relates the brightness of the distant source to the mutual coherence function (or visibility) via the 2D Fourier transform in a convenient set of coordinates for radio astronomy.

The Flat Sky Approximation and Its Limitations

In the above equation, we made one implicit assumption – that we are working in only two dimensions. This, of course, is not true.

In reality, the van Cittert-Zernicke theorem should be written in terms of *(u,v,w)* coordinates, rather than just *(u,v)*. The full (idealized) measurement equation can thus be written as:

$$V(u,v,w) = \iint I(l,m) e^{-2\pi i(ul+vm+w\sqrt{1-l^2-m^2})} dl dm \tag{3.6}$$

The next step is to assume that l and m are small, such that $\sqrt{1-l^2-m^2} \approx 1$, allowing the $e^{-2\pi iw}$ term to be removed from the integral by applying the proper phasing to the measured visibility and the measurement equation to be simplified to a 2D Fourier transform sampled in the *uv*-plane. This procedure is called the *flat-sky approximation*.

This approximation works well for many applications in astronomy, particularly in the observation of point sources or small extended sources in the sky (up to about ±10° or so,

where $l \equiv \sin\theta \approx \theta$). However, as the observed area in the sky gets larger, it becomes impossible to apply an absolutely correct phasor to the 2D integral, and the w-term instead introduces a spatially varying departure from the 2D Fourier transform the further from the phase center you are.

So, obviously, in the case where you're trying to use an interferometer to observe a global phenomenon (such as the reionization global signal), the flat sky approximation simply won't do. If we want to continue to use the 2D Fourier transform (spoiler alert: we do), the we must find a way to correct for this spatial variance.

3.2 Spatial Modes and Interferometric Sensitivities

As mentioned above in Section 3.1, interferometry gives you sensitivity to different spatially varying modes based on the physical separation of the antennas or telescope reflecting dishes making the observation. The bigger the separation, the faster the spatial variation observed on the sky, and therefore the higher resolution/smaller the object that can be observed.

It is through this knowledge that we are able to construct instruments that are specifically tuned to different spatial scales. For example, astronomers (and the general public) are fascinated by black holes and want to observe their inner workings. Black holes are very compact objects in the sky, so to be able to resolve them takes incredibly high resolution observations. Under the Rayleigh criterion (Eq. 3.7), radio astronomers can achieve fine resolution (i.e. small θ) by using high frequencies (i.e. small λ, of the order of less than a millimeter) and very large baselines (i.e. large B, on the order of thousands of kilometers).

$$\theta = \lambda/B \tag{3.7}$$

Alternately, if one wanted to observe fluffy galactic clouds or other extended structures, they would instead prefer to construct an interferometer using closely packed antennas and lower frequencies.

By constructing an array using a combination of differing baselines, one can fill in the sampling of the uv-plane. With complete sampling of the uv- plane, one can perform a simple 2D Fourier transform and perfectly recreate the image plane. This relationship between spatial frequency and images, or visibility and brightness, is known as the *spatial Fourier transform*, and is the backbone of all radio interferometry, from the reconstruction of cosmological power spectra all the way to the sophisticated synthesis imaging techniques described above.

In reality, of course, it is impossible to completely sample the uv-plane and recover a perfect image. We must therefore design our instruments to be maximally effective at the observations we wish for them to make. In the cases of general purpose instruments like the Very Large Array (VLA), that means designing the instrument to be very flexible – covering a broad range of frequencies, minimizing redundancy in the baselines, and using different array configurations to better sample different regions of the uv-plane.

However, for smaller scale instruments, astronomers generally wish to build something which is very specifically tailored for the observation they want to be making, leading to creative and highly unique array configurations that make use of the spatial Fourier transform to the best of their ability.

Spatial Fourier Transforms

Much as we can think of the relationship between time and frequency as a Fourier pair, we can also relate the physical separation of the antennas (i.e. the "geometric time delay" τ_g) and the spatial frequency.

Consider the variable u, which is defined as the baseline separation of two antennas measured in wavelengths in Eq. (3.2). Based on Eq. (3.1), we also know that $R_C \approx \cos(2\pi ul)$, meaning that the number of whole fringes imposed across the sky for any given separation will be $N_f = 2u$.

This in turn means that a pair of antennas separated by u wavelengths will be most sensitive to objects with an angular scale of about $\theta = 1/u$, according to Eq. (3.7).

One can relate this to the idea of spherical harmonics, with the harmonics providing us the (l, m) coordinates of our observed brightness, providing us some context for the second member of our spatial Fourier pair. We can thus start visualizing the physical meaning of "spatial variance" and "spatial frequencies".

3.3 Observing the Spatial Monopole with an Interferometer

At this point, you may be wondering how exactly we intend to use an interferometer to observe a spatially invariant signal. Everything we have stated above indicates that interferometers see *changing* signals – they observe the spatial variance that they are sensitive to based upon the separation of the antennas and the frequency they are observing at. They are inherently AC circuits. The one thing they are explicitly not meant to do is to observe what is effectively a DC tone.

So what the *hell* are we doing?

Well, it turns out there's a couple of things in our favor here. The first thing, as addressed in Presley et al. (2015), is that we're on earth and can't actually see a monopole from the sky – the horizon gets in the way. Furthermore, the antenna itself has a directionally dependent beam, introducing an additional layer of spatial variance. Therefore, what in reality is a monopole signal from the entire universe is instead observed as a *dipole* signal. And a dipole signal, with it's slowly varying signal across the sky, doesn't necessarily integrate to zero and therefore may be observable with an interferometer.

That being said, a dipole signal still isn't easily observable with an interferometer – it's only one cycle of variation across the sky, and with factors like beam shape, it can be hard to tell what's sky variation vs. other factors.

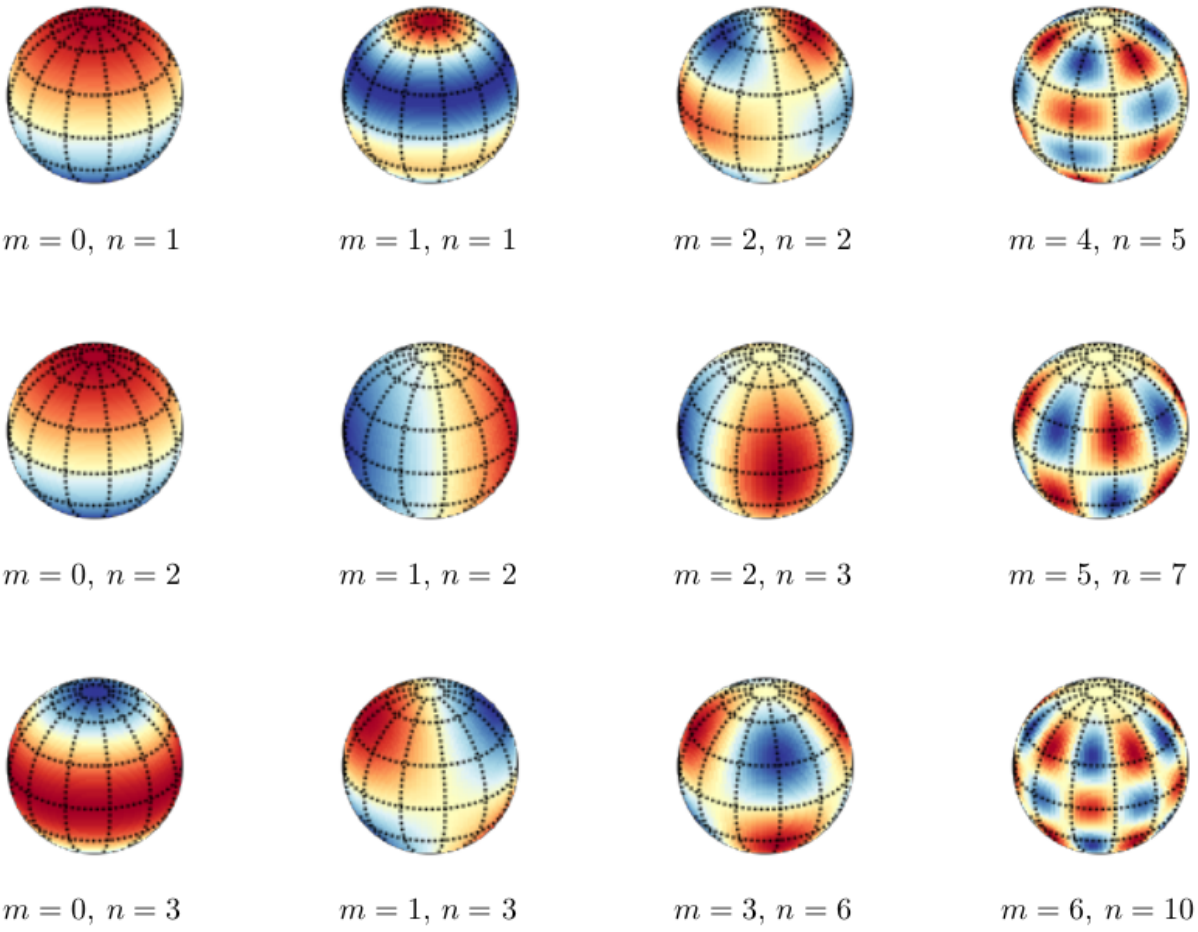

Figure 3.1: MAKE A FIGURE SHOWING SPHERICAL HARMONICS LMAO

What we need to do is artificially push our monopole term into higher modes – modes that we are in control of. Or, in Fourier terminology, we need to apply a top-hat function to our monopole signal.

In doing so, we will generate a visibility sensitivity in the shape of a sinc function – meaning we will have sensitivity to our monopole term in many Fourier modes, rather than just in the $(0, 0)$ or $(0, 1)$ modes. If we control the shape of the top hat imposed, then we know the shape of the sinc function, meaning we can calibrate exactly what our monopole sensitivity should be at any given point in the uv-plane.

So now the question is simply how can we raise the horizon that our antennas see? One option would be to literally raise the horizon – either find or manufacture a deep valley for them to reside within. This would probably be challenging to do well – digging a valley for the whole array would undoubtedly be expensive, and it'd be very hard to find a

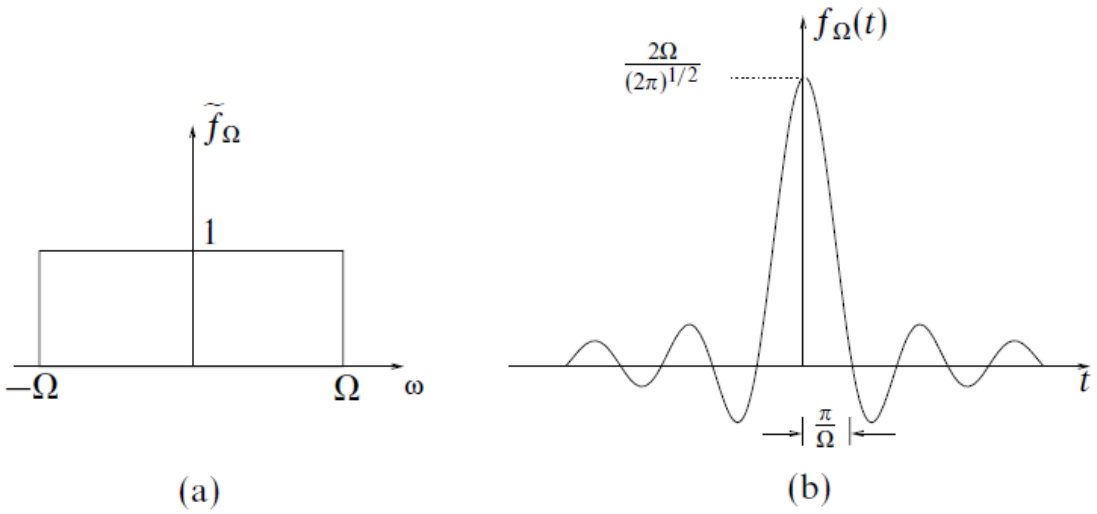

(a) A Fourier transform showing a rectangular distribution of frequencies between $\pm\Omega$; (b) the function of which it is the transform, which is proportional to $t^{-1}\sin\Omega t$.

Figure 3.2: MAKE A FIGURE SHOWING TOP HAT-SINC FOURIER RELATIONSHIP LMAO

naturally occurring, rotationally symmetric valley (particularly one deep enough to actually meaningfully raise the horizon of our antennas).

So we must find a way to artificially raise the horizon of our antennas. Moreso, as described in Venumadhav et al. (2016), we must either allow our antennas to freely cross-talk (thereby eliminating the vast majority of benefits gained from using an interferometric setup) or we must introduce a source of noise from lossy components (e.g. the ground or other signal absorbers, rather than reflectors or transmitters) in order to maintain a sensitivity to the global signal. As described in Section 3.1, the more closely spaced your elements, the larger the spatial scales your instrument will be sensitive to. We therefore know that we are going to be using a very closely packed array, which will make our system very prone to cross-talk. If we want to avoid that, then we'll have to find some way to ensure that the antennas don't see each other in addition to seeing less of the sky.

All of which leads us to the construction of thin absorptive walls between the antennas – introducing a new horizon in how the antenna sees the sky and maintaining the independence of each antenna's signal from its very nearby neighbors. In order to maximize our sensitivity to the global signal, we will want the absorbers used to be highly efficient at dissipating energy across our frequency spectrum (Venumadhav et al. 2016). This will provide us will

a strong "edge" in how our antennas see the sky, in turn creating maximal Fourier leakage into higher modes and best enabling us to make a successful observation of the reionization monopole signal.

Chapter 4

Absorber – A New Approach to Monopole Interferometry

4.1 Practical Instrumentation

4.2 Manipulating the Spatial Monopole

4.3 Initial Results

Chapter 5

Overview of the Theory of HYPERION

5.1 Simulation

The basis of our simulation lies in the calculation of a visibility using Eq. (5.1).

$$V(u,v) = \int A(\hat{s}) \cdot T_{sky}(\hat{s})\ e^{-2\pi i \frac{\vec{b}\cdot\hat{s}}{\lambda}} d\Omega \tag{5.1}$$

From this equation, we have three parameter spaces to play in: the beam of the antenna $A(\hat{s})$, the brightness and spatial behavior of the sky $T_{sky}(\hat{s})$, and the baseline vector $\vec{b}$. For ease of organization, we'll now split our discussion into two parts, sky characteristics vs. system characteristics.

Sky Characteristics & Parameters

At present, our goal is to better understand how an interferometer receives signal from a monopole sky, so we're only considering skies without any spatial variation. However, while we are only inputting spatially flat maps into the simulation, spectral variation across our science band is an open variable that we consider. The simulation has functions for both spectrally-flat (for calibration and verification purposes) and synchrotron-characteristic sky maps, using Eq. (5.2) as our basis for calculating brightness temperature as a function of frequency.

$$T(\nu) = T(\nu_{150})\Big(\frac{\nu}{\nu_{150}}\Big)^{-\beta} \tag{5.2}$$

System Characteristics & Parameters

This leads us to the characteristics of our interferometer itself. Within this framework, there are two key areas of interest to us: how our sensitivity to the monopole varies with the separation between antennas, and how it changes in the presence of different absorber structures and materials. Another way of viewing it would be: how do the characteristics of the individual elements and of the array design affect our ability to make this measurement.

Let us first consider the array design, i.e. baseline separations. For this simulation, we import a model array using the AIPy AntennaArray framework, which enables us to carry around an array with known geometry and baseline separations, along with individual antenna beam patterns and accessible frequencies. With this information and the previously made sky maps, we are now able to calculate our visibilities across many frequencies by using Eq. (5.1).

Intuitively, we expect that the sensitivity to the global signal will be maximized with the smallest baseline separations, which correspond to a position in the *uv*-plane close to the origin, or the zero-spacing mode. The trade-off of this, from a design perspective, comes in the difficulty of ameliorating cross-talk in a densely packed array. We want to optimize our array design to space our antennas as loosely as possible while also maintaining workable sensitivity to the monopole term, as this will best enable us to mitigate systemic problems in our instrument and perform a successful experiment.

The AntennaArray framework also enables us to carry around models of the beams of the antennas, which is a convenient way to import absorbers into the simulation. Essentially, within the context of the simulation, the absorbers act as a modification term on the beam pattern, changing the way that each individual antenna sees the sky. This works as follows:

To start, we need a beam. HYPERION uses SARAS-style fat dipole antennas in our instrument, which means we will be using a frequency-invariant dipole beam pattern in our simulation to match (Patra et al. 2013). This is the base beam model used throughout the simulation, calculated using Eq. (5.3).

$$A(\theta, \phi, \nu) = \cos\left(\frac{\frac{\pi}{2}\cos\theta}{\sin\theta}\right) \tag{5.3}$$

The next step is to add the absorber, which we do via modification of the AIPy Antenna beam. The absorber structure in our simulation is essentially a cylindrical wall of uniform height centered around each antenna, so that the antenna sees a rotationally symmetric structure. The parameters we can play with are the absorptivity of the material (i.e. how much attenuation does the absorber provide at each frequency), the height of the absorber walls, and how smooth the transition from absorber to sky is. This calculation is done using Eq. (5.4),

$$B(\theta, \phi, \nu) = \left[10^{\alpha(\nu)/20}\left(\frac{1}{2} + \frac{1}{2}\tanh\left(\frac{\theta - (\frac{1}{2} - \theta_0)}{a}\right)\right) + \left(1 - \left(\frac{1}{2} + \frac{1}{2}\tanh\left(\frac{\theta - (\frac{1}{2} - \theta_0)}{a}\right)\right)\right)\right] \tag{5.4}$$

where $\alpha(\nu)$ is the absorptivity by frequency of the absorber, θ_0 is the cutoff angle of the structure (i.e. θ_0 is the height of the absorber walls), and a is the smoothing parameter that blends the transition between the absorber and the sky.

This term is then combined with the Antenna beam, giving us Eq. (5.5).

$$A'(\theta, \phi, \nu) = A(\theta, \phi, \nu)B(\theta, \phi, \nu) \tag{5.5}$$

Calculating Visibilities by Baseline Separation

One of the fundamental constructs of the theory of astronomical interferometry is that samples spatial variance on the sky. Interferometers, by nature, are not designed to observe global light sources. Rather, interferometers excel at observing differences – a star or other point source will have light in one place and no light everywhere else, galaxies will have clumpy, fluffy light in some places but not all places. The interferometer can be built and designed to observe some scales better than others, and can tease out these differential light sources with great success.

So one might reasonably be surprised to hear that we are taking an interferometer and trying to do the one exact thing that it is, theoretically, unequipped to handle: trying to observe a global average phenomenon on the sky.

Chapter 6

Sensitivity to the Monopole Sky

6.1 Simulated

lay out the case that absorber helps us maximize interferometric sensitivity to monopole, lay out the case that we can use the characteristics of this sensitivity to potentially help us pick out monopole vs. higher order terms (some kind of filtering around sensitivity vs. u mode)

As can be easily seen in Figures 6.1 and 6.2, all interferometers have a non-zero sensitivity to the monopole mode of the sky. As the number of wavelengths of separations increases, that sensitivity also quickly evaporates.

now speak to absorbers that we tried and how they all performed. show results of monopole sky with absorber, compare to without absorber and show that there is greater sensitivity

We can also begin to see a characteristic shape of the sensitivity in the uv-plane, with peaks and nulls placed at regular intervals in uv-space. The predictability of this shape could allow us to use it as a calibration tool, if properly understood. In particular, it could be a valuable way to remove leakage from non-monopole terms into our signal. Given that this characteristic shape derives only from the monopole sky and the shape of the beam, we know that any observational deviations in this shape must come from the sky rather than the system. Therefore, it may be possible to use this information as a way to

Additionally, this shape enables us to do some weighting of our observational data. By knowing exactly what modes we expect to see the monopole term at its brightest and dimmest, we can properly weight and interpret our data at each mode and frequency, enabling us to better compare data points at different points in uv-space and frequency.

6.2 Recovered

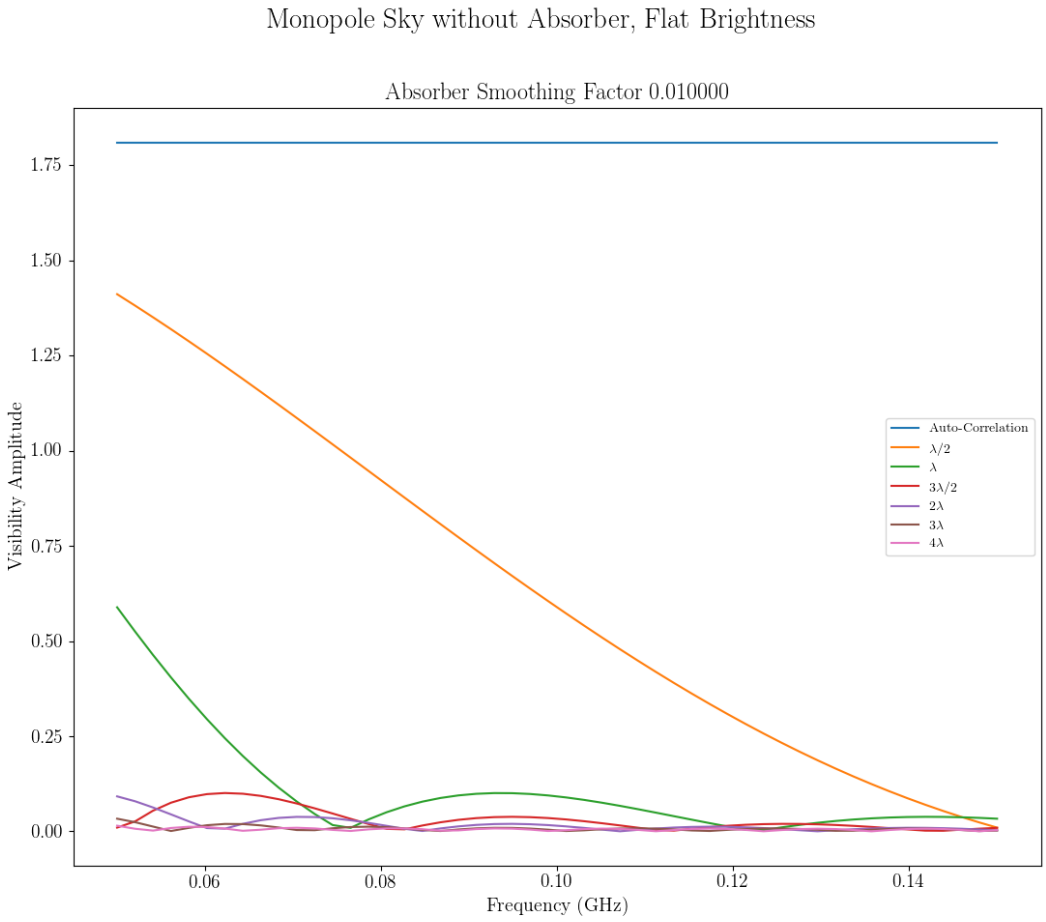

Figure 6.1: Shown here is the absolute value of the visibility of a spectrally flat monopole sky with no absorber walls versus frequency. As can be seen already, the interferometer does have non-zero sensitivity to the monopole, though it is plainly clear that the autocorrelation term (shown in blue) is more sensitive than any of the non-zero interferometric baseline pairings.

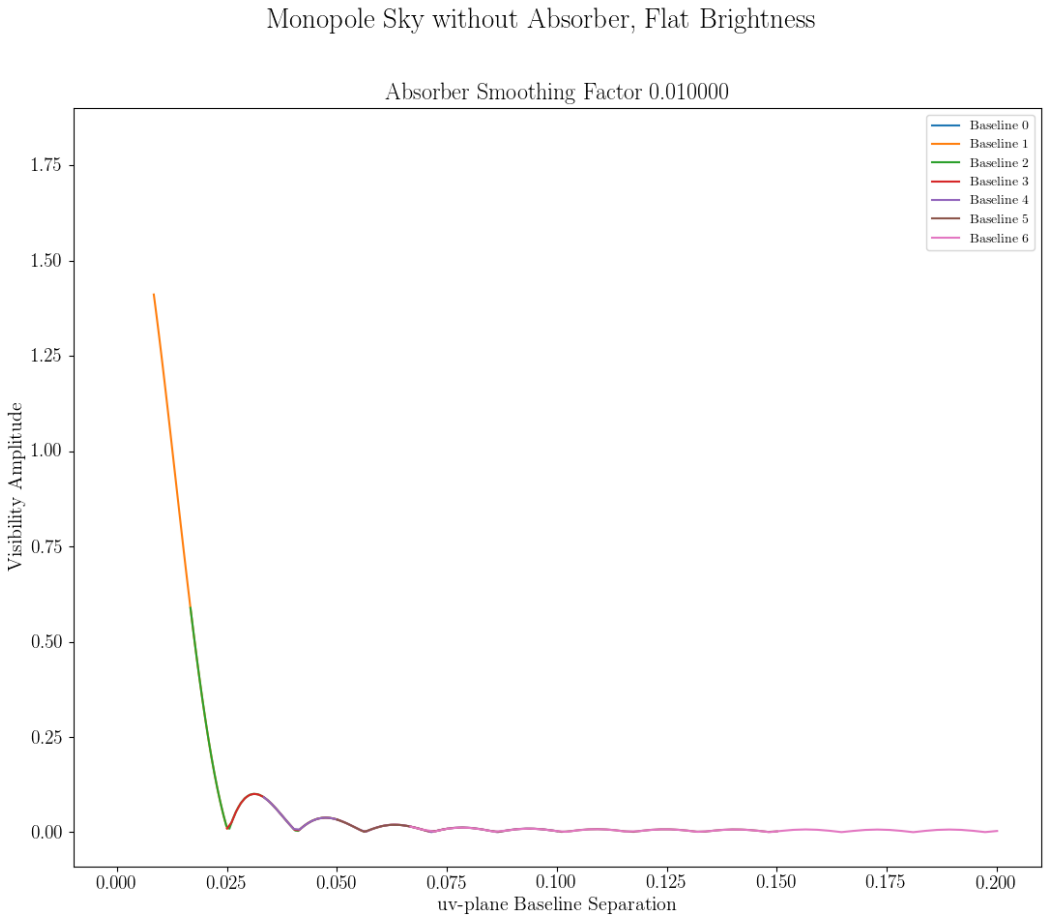

Figure 6.2: REMAKE THIS FIGURE Shown here is the absolute value of the visibility of a spectrally flat monopole sky with no absorber walls versus uv-baseline. As can be seen already, the interferometer has a non-zero sensitivity to the monopole at non-zero baseline separations.

Chapter 7

Conclusion

review all chapters and results, but pithier

Bibliography

Bowman, J. D., & Rogers, A. E. E. 2010, Nature, 468

Bowman, J. D., Rogers, A. E. E., Monsalve, R. A., Mozdzen, T. J., & Mahesh, N. 2018, Nature, 555

DeBoer, D. R. e. a. 2017, Publications of the Astronomical Society of the Pacific, 129

Furlanetto, S. R., Oh, S. P., & Briggs, F. H. 2006, Physics Report, 433

Gardner, J. P. e. a. 2006, Space Science Reviews, 123

Kundert, K. 2016, The Relationship Between System Temperature and Sky Beam Coverage, Memo 1, HYPERION

Patra, N., Subrahmanyan, R., Raghunathan, A., & Shankar, N. U. 2013, Experimental Astronomy, 36

Presley, M. E., Liu, A., & Parsons, A. R. 2015, The Astrophysical Journal, 809

Pritchard, J. R., & Loeb, A. 2010, Physical Review D, 82

—. 2012, Reports on Progress in Physics, 75

Venumadhav, T., Chang, T.-C., Doré, O., & Hirata, C. 2016, The Astrophysical Journal, 826

Zaroubi, S. 2012, in The First Galaxies, – Theoretical Predictions and Observational Clues, ed. T. Wiklind, B. Mobasher, & V. Bromm (Springer), 45–101